ACS APPLIED MATERIALS & INTERFACES

Research Article

www.acsami.org

Graphene Quantum Dot Hybrids as Efficient Metal-Free Electrocatalyst for the Oxygen Reduction Reaction

Yong Liu and Peiyi Wu*

State Key Laboratory of Molecular Engineering of Polymers, Department of Macromolecular Science, and Laboratory of Advanced Materials, Fudan University, Shanghai 200433, People's Republic of China

Supporting Information

ABSTRACT: The doping of heteroatoms into graphene quantum dot nanostructures provides an efficient way to tune the electronic structures and make more active sites for electro-catalysis, photovoltaic, or light emitting applications. Other than the modification of chemical composition, novel architecture is very desirable to enrich the research area and provides a wide range of choices for the diverse applications. Herein, we show a novel lotus seedpod surface-like pattern of zero-dimension (0D) seed-like N-GODs of ca.3 nm embedded on the surface of a two-dimension (2D) N-GQD sheet of ca.35 nm. It is demonstrated that different photoluminescence (PL) could be tuned easily, and the novel multidimensional structure displays excellent performance toward oxygen reduction reaction in alkaline solutions. Thus, the fabricated N-GQD hybrids show bright perspective in biomedical imaging, biosensors, and conversion and storage of energy.

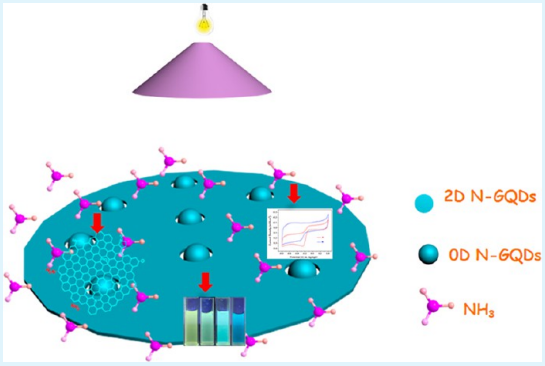

KEYWORDS: *graphene quantum dots, architecture, photoluminescence, oxygen reduction reaction*

INTRODUCTION

The development of low-toxic, eco-friendly, and chemically inert fluorescent materials[1] is integral to the progress of emerging fields such as nanobiomedicine,[2] biotechnology,[3] fuel cells,[4] and optoelectronics.[5] In this aspect, graphene quantum dots (GQDs),[6] a rising star in the graphene family, have recently been subjected to extensive research in materials science and engineering. In contrast to quasi-spherical carbon dots with size below 10 nm, GQDs are defined as the graphene sheets with lateral dimensions less than 100 nm in single, double, and a few layers (3 to <10 layers).[7] By far, a variety of synthetic methods have been developed which were generally categorized into two major approaches, known as top-down and bottom-up methods, in which the former refers to the cutting of graphene sheets into GQDs, such as acidic or electrochemical oxidation,[8,9] hydrothermal treatment,[10] and microwave-assisted and photo-Fenton reaction methods,[11,12] while the later is the solution chemistry method, during which the GQDs are formed from molecular precursors.[13−15] As an attractive material distinct from the "classic" photoluminescent nanoparticles (NPs) (e.g., quantum dots, dye-doped NPs, and rare earth-based NPs) as well as silicon quantum dot, the GQDs not only exhibit interesting size- and wavelength-dependent down-conversion and up-conversion photoluminescence (PL) but also inherit the superior performance from graphene, such as large specific surface area, excellent electrical conductivity, and good thermal conductivity.[16]

Although PL mechanisms from the quantum size effect along with different emissive traps and two-photon induced excitation on the GQD surface have been widely studied experimentally and theoretically over the last several years,[17,18] the significant technological potentials of GQDs have just started to emerge.[19−21] Therefore, to explore the potential application and discover new phenomena and unexpected properties of GQDs, one possible route is to modulate its property by chemical doping and modification. Qu et al.[22] electrochemically prepared N-functioned GQDs with N/C atomic ratio of ca. 4.3%. Unlike their green luminescent N-free counterparts, N-GQDs emitted blue luminescence due to the relatively strong electron withdrawing ability of pyridinic-N and pyrrolic-N atoms in the N-GQDs; they also possessed an electro-catalytic activity for ORR. Li et al.[23] demonstrated that other than the mostly focused hypothetical correlation between the catalytic activity and the bonding configuration of nitrogen atoms in the carbon skeleton, the nitrogen-functioned graphene dots have highly size-dependent electro-catalytic activity. Okamoto et al.[24] proposed that directly bonding primary amino group at the edge of GQDs could induce its molecular orbital resonance with the delocalized π orbital of GQDs, thereby endowing them with high efficiency and wide tuning ability of narrow PL. In another perspective, Jin et al.[25] reported that the charge transfer between amino groups and GQDs can tune the band gap of the GQDs, resulting in the shift of PL.

Received: January 31, 2013
Accepted: March 26, 2013
Published: March 26, 2013

In despite of the aforementioned significant work aimed at changing the chemical composition of GQDs by N atom functionalization, all these processes are difficult to scale up, which limits their practical use. Moreover, expanding the scope from purely chemical modification of GQDs to architecture engineering, by combining the intrinsic properties of GQDs with fascinating structure advantages (e.g., efficient ion or molecule transport), could significantly broaden the field of GQD material capability; however, to date, novel architecture has been scarcely reported for GQDs,[26] while it is widely reported for various other materials, such as Ag nanocube,[27] Au nanocage,[28] york-shell TiO_2,[29] and two-dimension (2D) mesoporous graphene sheet.[30] Recently, Li et al.[31] employed colloidal graphene quantum dots as a model substrate for carbon materials to study metal−carbon interaction; they directly proved the covalent interaction between the Pd particles and pristine graphene by infrared (IR) spectroscopy. Thus, we believe that GQDs, the smallest size in the graphene sheet family, could still be served as a unique support substrate for hierarchical architecture engineering. In our work, we prepared a kind of N-GQDs with average size of 35 nm (N-GQDs-35) at a gram scale by refluxing the N-containing PAN-based carbon fiber in HNO_3 solution. Inspired by the GQDs extracted through the ammonia-mediated bond-scission reaction from oxidized graphene sheet (GO), we present a new structure by the use of low-concentration ammonia as a mild "utility knife" to facilely carve lotus seedpod surface-like patterns of seed-like zero-dimension (0D) N-GODs of ca. 3 nm embedded on the surface of 2D N-GQDs-35 sheet as a "canvas". Nitrogen- and oxygen-rich functional groups enable them to be stable in water and several polar organic solvents, compared with the hydrothermal aggregation and precipitation of GO in the same process.[32] Moreover, this architecture offers a unique combination of two types of GQD hybridization and more active sites induced by defects and holes on the surface and N heteroatom functionalization, thus allowing for tailored PL and very efficient catalytic activity to ORR in alkaline media. The detailed fabrication process is illustrated in Scheme 1. As a future perspective, the N-GQDs show bright promise in biological imaging, disease diagnosis, fuel cells, and biosensors.

EXPERIMENTAL SECTION

Materials. T800 was purchased from Toray Inc. Graphite powder was obtained from Aladdin Reagent Co. Ltd. All other reagents are of analytical grade and used without further purification.

Scheme 1. Strategy for the Synthesis of N-GQDs

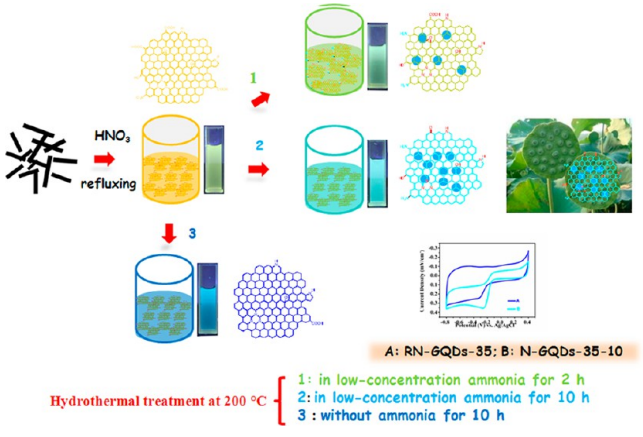

Preparation of N-GQDs-35. PAN-based carbon fiber powder (2.0 g) was heated at 500 °C for 0.5 h in a flow of Ar to eliminate the sizing agent on the surface. The as-received powder was added to 200 mL of concentrated HNO_3 under ultrasound for 2 h; then, the suspension was maintained at 130 °C for 24 h under vigorous stirring before evaporating the water and nitric acid by vacuum distillation. The obtained product was redispersed in 200 mL of water, followed by adjusting its pH to 7 with ammonia aqueous solution (28 wt %), and further dialyzed in a dialysis bag (retained molecular weight: 1000 Da) for 2 days. The obtained N-GQD supernatant was then dried in a rotary evaporator. A reddish-brown solid (ca. 1.0 g, 50%) was obtained and dried in vacuum at 50 °C for 12 h.

Hydrothermal Treatment of N-GQDs. Five milliliters of the above N-GQD solution (5 mg/mL) and 50 μL of ammonia aqueous solution (28 wt %) were transferred into a Teflon-lined stainless-steel autoclave (25 mL capacity) and held in an oven at 200 °C for 2, 6, 10, and 14 h (the corresponding products are named as N-GQDs-35-2, N-GQDs-35-6, N-GQDs-35-10, and N-GQDs-35-14, respectively). After reaction, the hydrothermally treated N-GQD powder was obtained on evaporating the solution in a rotary evaporator. The control sample RN-GQDs-35 was prepared without ammonia aqueous solution with the same method.

Characterization Methods. The transmission electron microscope (TEM) images were taken with a JEOL JEM-2100F microscope (Japan) equipped with electron diffraction. Field-emission scanning electron microscopy (FE-SEM) was performed on a Hitachi S-4800 electron microscope. Hydrodynamic diameter measurements were conducted by dynamic light scattering (DLS) with a ZEN3600 (Malvern, UK) Nano ZS instrument using He−Ne laser at a wavelength of 632.8 nm. Wide-angle XRD patterns were recorded on a Bruker D8 diffractometer (Germany) with Ni-filtered Cu Kα radiation. Ultraviolet−visible (UV−vis) absorption spectra were measured on a UV-3150 spectrometer (Shimadz, Japan). Raman spectra were collected on a Renishaw in Via Reflex micro-Raman spectrometer with 633 nm laser excitation. The data acquisition time was usually 10 s, and peak intensities of samples were normalized to that of the silicon wafer at 520 cm^{-1}. Fluorescence spectra were recorded on an RF-5301PC spectrofluorometer (Shimadz). Atomic force microscopic (AFM) images were obtained using a Multimode Nano 4 in the tapping mode. For AFM observations, the samples were dispersed in the water (0.2 mg/mL) with the aid of ultrasonic treatment and then spin-coated onto freshly cleaved mica surfaces. X-ray photoelectron spectra (XPS) were measured by a Perkin-Elmer PHI5000C spectroscope with Mg Kα line as the excitation source.

Electrochemical Measurements. *Catalyst Preparation.* Graphene oxide (GO) sheets were synthesized by a modified Hummers method.[33] The as-prepared N-GQDs (25 mg) was mixed with 20 mL of GO aqueous solution (1.25 mg/mL) to form a homogeneous dispersion by slight ultrasonic treatment. The aqueous dispersion was then sealed in a 25 mL Teflon-lined autoclave and maintained at 200 °C for 14 h. This hydrothermal treatment will reduce the GO and allow the in situ formation of N-GQD decorated graphene sheets as catalyst.

Electrochemical tests such as cyclic voltammetry (CV) tests were measured on a computer-controlled potentiostat (CHI 660D) in a standard three-electrode cell under ambient condition. The working electrode was made from the N-GQDs/graphene catalysts and Nafion as a binder. Typically, 0.2 mg of a certain catalyst dispersed in 100 μL of water was mixed with 100 μL of a 0.5 wt % Nafion solution and ultrasonicated at room temperature for 10 min. Five microliters of the above-prepared catalyst ink was injected onto a polished glassy carbon electrode and dried at ambient conditions before electrochemical measurement. A Pt wire (0.5 mm in diameter) and Ag/AgCl were used as counter and reference electrodes, respectively. For ORR measurements, an aqueous solution of 0.1 M KOH was used as the electrolyte. N_2 or O_2 was used to purge the solution to achieve the O_2-free or O_2-saturated electrolyte solution. The rotating disk electrode (RDE) technique was employed to study the ORR activity and kinetics with a rotating speed of 400−1600 rpm. Koutecky−Levich equation

was used to analyze the number of electrons transfered in oxygen reduction.

$$\frac{1}{J} = \frac{1}{J_L} + \frac{1}{J_K} = \frac{1}{B\omega^{1/2}} + \frac{1}{J_K}$$

$$B = 0.62nFC_{O_2}D_{O_2}^{2/3}\nu^{-1/6}$$

In the Koutecky–Levich equation, J, J_L, and J_k are the measured current density, the diffusion-limiting current density, and the kinetic-limiting current density, respectively; ω is the angular velocity, F is the Faraday constant (96485 C mol^{-1}), D_{O_2} is the diffusion coefficient of O_2 in solution, ν is the kinetic viscosity (0.01 cm^2 s^{-1}), and C_{O_2} is the bulk concentration of oxygen.

RESULTS AND DISCUSSION

The starting PAN-based carbon fiber has an average diameter of about 18 μm, with length up to 300 μm, as shown in the scanning electron microscopy (SEM) image in Figure S1, Supporting Information. Nitric acid could react with many organic materials and all metals, except for the noble metals series and certain alloys. Upon specific reactions with carbon elements, which are considered in this work, it usually oxidizes them into their highest oxidation states, accompanied by forming nitric oxide (NO), nitrogen dioxide (NO_2), and carbon dioxide (CO_2).[34] Hence, it is utilized for the oxidative cutting of CF for making GQDs. The as-prepared N-GQDs are found to exhibit a high solubility in water and other polar organic solvents (DMF and DMSO) in the long-term homogeneous phase. Dynamic light scattering distribution of the N-GQD hydrodynamic diameter is shown in the inset of Figure 1a, revealing a relatively narrow size distribution with an average diameter of 35 nm (abbreviated as N-GQDs-35).

The high resolution TEM (HRTEM) image does not reveal any clear lattice fringes, indicating the amorphous nature of the N-GQDs-35. The N-GQDs-35 aqueous solution emits bright yellow PL excited by 365 nm lamp. Figure 2A presents an atomic force microscopy (AFM) image of the N-GQDs-35 on a mica substrate; it is found that the topographic heights of N-GQDs-35 are mostly between 0.5 and 1 nm (0.7 nm average height), suggesting single layered or bilayered in most of the 2D N-GQDs-35 sheet. In order to facilely carve out patterns on the surface of the N-GQDs-35 sheet without expensive devices or complicated manipulation, such as atomic force microscopy (AFM)[35] or e-beam,[36] ammonia, which could react with epoxy groups to form a primary amine and alcohols by nucleophilic substitution, is used in the preparation of GQDs by extraction of the sp^2 domains from the graphene oxide.[24] However, large mass ratio of ammonia/GO (e.g., 3-fold) is routinely used to completely peel off GQDs from graphene oxide,[24,37,38] eventually leading to the aggregation and precipitation of the formed graphene on the bottom while the product GQDs dispersed in the solution. In our work, small mass ratio of ammonia/N-GQDs (ca. 0.002) is employed, aimed to mildly carve the surface. Hydrothermal reaction at 200 °C is chosen owing to the most obvious PL change from yellow to cyan at this temperature under irradiation from a 365 nm UV lamp as an intuitively well-determined way (Figure S2, Supporting Information). Time-resolved experiments are subsequently adapted from 2 to 14 h at 200 °C. At 2 h, the PL changes from yellow to yellow-green. Compared with the smooth surface of N-GQDs-35, small "dark dots" appear on that of N-GQDs-35-2, accompanied by some curved N-GQDs-35-2 lamellas. The "dark dots" obtained are polycrystalline with a

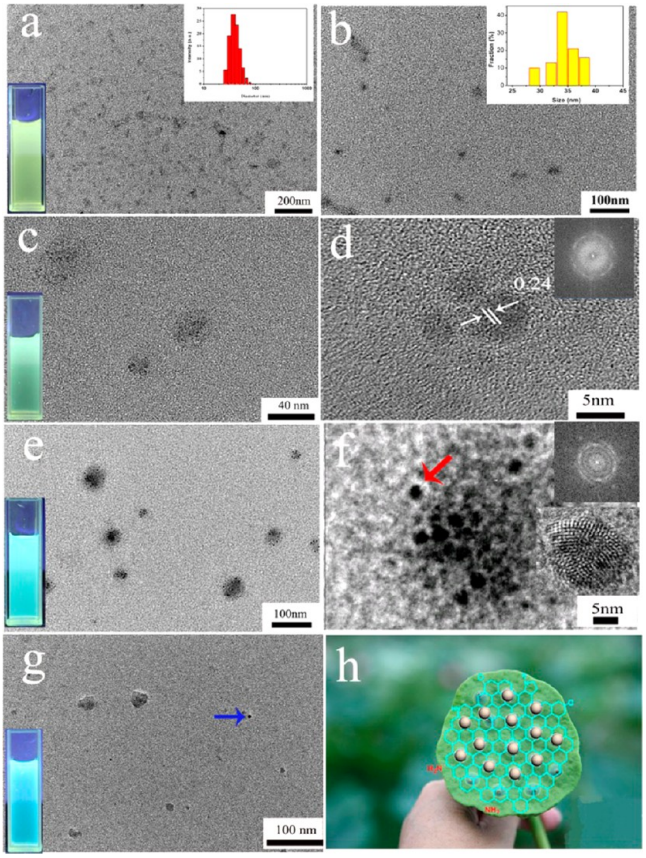

Figure 1. (a, b) TEM image of the as-prepared N-GQDs-35 under different magnifications. The insets in (a) and (b) show the dynamic light scattering distribution of the N-GQDs-35 hydrodynamic diameter and statistic size distributions of N-GQDs-35 from TEM. (c) TEM image of N-GQDs-35-2. (d) HRTEM and FFT image of N-GQDs-35-2. (e) TEM image of N-GQDs-35-10. (f) TEM image of single N-GQDs-35-10 NPs and hole is marked by a red arrow; inset is the HRTEM image of "dark dots" and its FFT image. (g) TEM image of N-GQDs-35-14. (h) A cartoon shows the structure of N-GQDs-35-10. Emission images of N-GQDs dispersed in water (inset of a, c, e, g) under irradiation from a 365 nm UV lamp.

lattice parameter of 0.24 nm (the FFT and HRTEM image in Figure 1d), corresponding to (1120) lattice fringes of graphene. At 10 h, the PL changes from yellow–green to cyan, and more "dark dots" are formed (Figure 1e). It is interesting to find that, different from the reported gradual disappearance of GO substrate as carbon source,[38] the support substrate (N-GQDs-35) has not yet disappeared, but concomitantly becomes "dark" and holes are leaved (red arrow); therefore, it is speculated that N-GQDs-35 may self-assemble due to $\pi-\pi$ stacking along with the appearance of dark dots in the process. The HRTEM image shows that the larger dark dots with an average diameter of 3 nm are highly polycrystalline (Figure 1f), which is in excellent agreement with high-quantity zero-dimensional (0D) graphene quantum dots prepared by the use of other routes.[25] The hybrid structure observed from HRTEM is like many 0D lotus seeds embedded on the surface of lotus seedpods. A cartoon in Figure 1h graphically illustrates the novel architecture of N-GQDs-35-10. Prolonging the reaction time to 14 h will cause the exfoliation of "0D lotus seed" (marked by a blue arrow in Figure 1g), leaving the further self-assembled N-GQDs-35-14.

To illustrate the size and height change of the novel structure in the scission and self-assembling process, their AFM

dx.doi.org/10.1021/am400415t | ACS Appl. Mater. Interfaces 2013, 5, 3362–3369

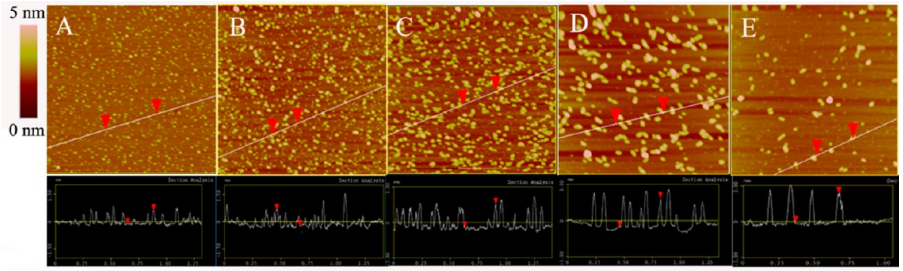

Figure 2. AFM images (upper row) and the corresponding height distribution images (bottom row) of N-GQDs-35 (A), N-GQDs-35-2 (B), N-GQDs-35-6 (C), N-GQDs-35-10 (D), and N-GQDs-35-14 (E).

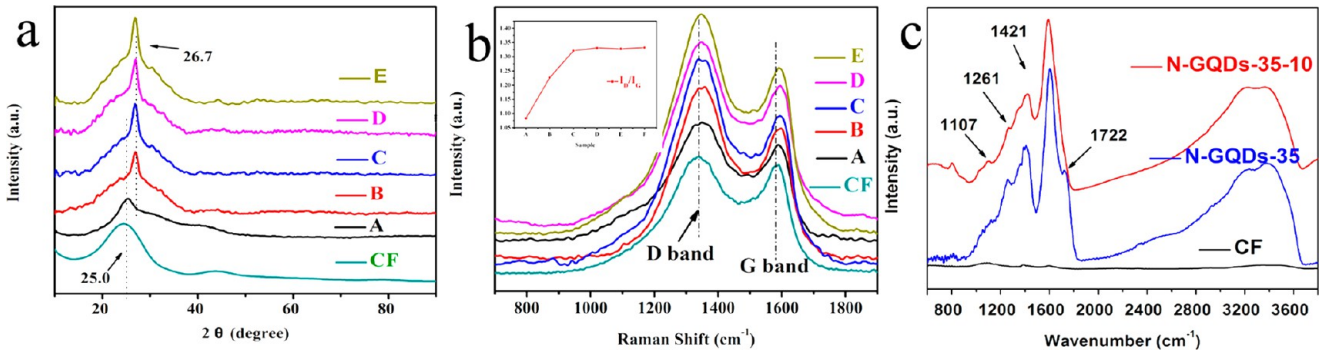

Figure 3. XRD patterns (a) and Raman spectra (b) of CF, N-GQDs-35 (A), N-GQDs-35-2 (B), N-GQDs-35-6 (C), N-GQDs-35-10 (D), and N-GQDs-35-14 (E). Inset is I_D/I_G. The typical FTIR spectra (c) of CF, N-GQDs-35, and N-GQDs-35-10.

observations are displayed in Figure 2. At 2 h, the height of N-QDs-35-2 is improved to 1.3 nm but shows little deviation in size (Figure 2B), indicating alteration of surface microstructure. From 6 to 10 h, both the size and heights increase steadily to ca. 2.5 and 58 nm, respectively, meaning that the N-GQDs-35-10 is mostly three-layered. After 14 h, the height and size slightly changes and stabilizes at ca. 3 and 60 nm, respectively, corresponding to 4−6 layers. In addition, it is observed that the amount of N-GQDs distributed on the surface of mica decreases by time at the same sample concentration, revealing that many small N-GQDs participate in the assembly process.

X-ray diffraction (XRD) is an important tool for determining the structure change of GQDs. As shown in Figure 3a, the N-GQDs-35 has a broader (002) peak centered at around 25.0°. After hydrothermal reaction, the N-GQDs show a narrower (002) peak, and the peak has been shifted to 26.7° with a *d*-spacing value of 0.33 nm. This decrease in interlayer spacing is indicative of the gradual formation of well-ordered graphite structure through $\pi-\pi$ interactions due to the removal of oxygen functionalities, and the broader peak is assigned to the disorderly assembled N-GQDs-35. Generally, hydrothermal reaction in the presence of ammonia solution not only cuts sp^2 clusters in graphene sheets into GQDs but also adds N atoms in the carbon skeleton. Raman spectroscopy, a powerful and nondestructive tool to verify the structural integrity of carbon-based structures, is employed to gather information regarding these defects. Raman spectra of the original CF and N-GQDs are included in Figure 3b. In N-GQDs-35, the peaks at 1348 and 1588 cm^{-1} are attributed to the defect induced D band and the first-order scattering of the E_{2g} mode for sp^2 carbon lattice (G band), respectively. Commonly the D peak/G peak intensity ratio (I_D/I_G) could be served as a convenient measurement of the amount of defects in graphitic materials. In the present study, I_D/I_G is enhanced substantially (CF: 1.08→N-GQDs-35: 1.22→N-GQDs-35-10: 1.32) and a broader D band is observed, suggesting more defects generated and concomitant intercalation of N atoms into the conjugated carbon backbone, disturbing the N-GQD surface structure. The G band of N-GQDs-35-10 shows red shift to 1596 cm^{-1}; the red shift of G bands is attributed to the restoration of sp^2 as new graphitic domains that are small in size but numerous according to the previous studies.[39] The molecular structure of N-GQDs is further investigated by the FTIR spectroscopy. As shown in Figure 3c, other than the disappearance of the COOH stretching vibration peak at 1722 cm^{-1}, C−O (epoxy) stretching vibration peak at 1261 cm^{-1} decreases dramatically, which is consistent with previous reports that epoxy groups could serve as chemically reactive sites for the rupture of the underlying C−C bonds. However, the N-GQDs-35-10 still shows an intensive C−O (alkoxy) stretching peak at 1107 cm^{-1} and a C−O (carboxy) deformation peak at 1421 cm^{-1}, which enable their high solubility in water. On the basis of above-mentioned TEM, AFM, XRD, Raman, and FTIR results, it follows that a water-soluble multidimentionl (2D and 0D) hybrid structure with many holes and defects has been realized by the hydrothermal reaction in small mass ratio of ammonia/GQDs.

PL and UV−vis absorption spectroscopic methods are used to explore the optical properties of the N-GQDs. The quantum yield of our prepared N-GQDs-35-10 was about 5.3%, comparable with other reported luminescent QDs.[40] Meanwhile, consistent with the change of PL observed by the naked eye under irradiation from a 365 nm UV lamp in the hydrothermal process, the maximal emission peak blue shifts from 525 to 484 nm with increasing hydrothermal time in the presence of the low-concentration ammonia solution and the intensity of PL reaches a maximum at 10 h in the whole process. UV−vis absorption of N-GQDs is shown in Figure 4b;

dx.doi.org/10.1021/am400415t | ACS Appl. Mater. Interfaces 2013, 5, 3362−3369

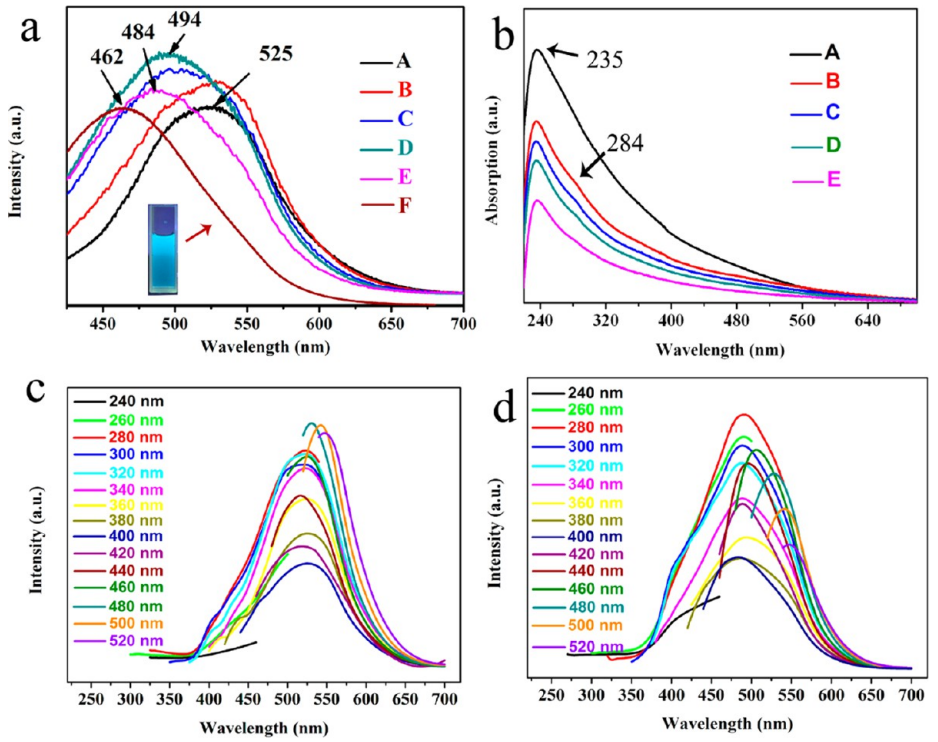

Figure 4. PL spectra (a) of N-GQDs-35 (A), N-GQDs-35-2 (B), N-GQDs-35-6 (C), N-GQDs-35-10 (D), N-GQDs-35-14 (E), and the control RN-GQDs-35 (F) excited at 365 nm; inset is emission images of the control under irradiation from a 365 nm UV lamp. UV−vis absorption (b) of N-GQDs-35 (A), N-GQDs-35-2 (B), N-GQDs-35-6 (C), N-GQDs-35-10 (D), and N-GQDs-35-14 (E). The typical PL spectra of the N-GQDs-35 (c) and N-GQDs-35-10 (d) at different excitation wavelengths.

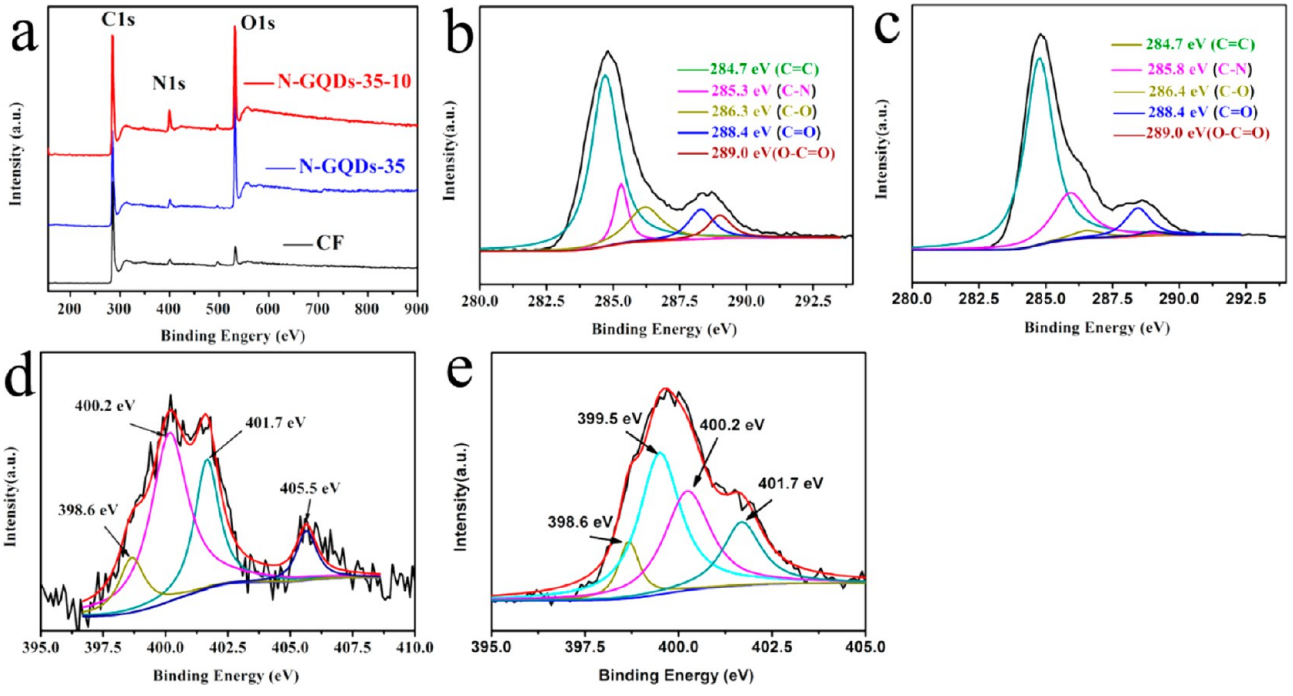

Figure 5. XPS survey spectra (a) of CF, N-GQDs-35, and N-GQDs-35-10. High-resolution C_{1s} and N_{1s} peaks of N-GQDs-35 (b, d) and N-GQDs-35-10 (c, e).

in N-GQDs-35, a typical absorption peak at ca. 235 nm could be observed, which is assigned to the $\pi-\pi^*$ transition of aromatic sp^2 domains. After hydrothermal treatment, different from the previous report that hydrothermal treatment of GO will increase the fraction of strongly localized sp^2 sites, thereby improving absorbance, in our work, the absorption intensity at 235 nm dramatically decreases, and a new peak at 284 nm appears; similar results have been reported for the hydrothermally prepared GQDs with varying the average size of GQDs from 5 to 35 nm. The peak energy of the absorption

dx.doi.org/10.1021/am400415t | ACS Appl. Mater. Interfaces 2013, 5, 3362−3369

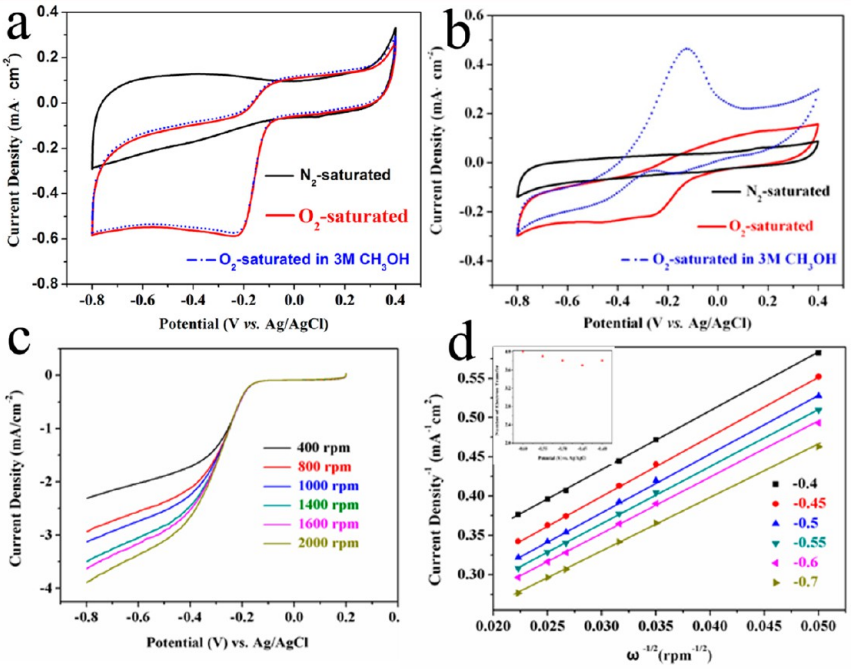

Figure 6. (a, b) CVs of (a) N-GQDs-35-10/graphene and (b) commercial Pt/C on a GC electrode in N_2-saturated 0.1 M KOH, O_2-saturated 0.1 M KOH, and O_2-saturated 3 M CH_3OH solutions. (c) Rotating disk electrode (RDE) curves for N-GQDs-35-10/graphene in O_2-saturated 0.1 M KOH with different speeds. (d) The Koutecky–Levich plots derived from the RDE measurements. The inset shows the dependence of n on the potential.

spectra monotonically decreases due to quantum confinement effect.[41] In our work, we tentatively speculate that new sp^2 clusters in N-GQDs-35 are formed during the hydrothermal reduction and some clusters are carved out and packed to form highly polycrystalline N-GQDs through $\pi-\pi$ stacking. As time goes by, the N-GQDs-35 could self-assemble and the small GQD aggregates form a large size of GQDs, resulting in the decreased absorption and red-shift of the absorption peak. A PL study is then carried out, as shown in Figure 4c,d; all of the obtained GQDs are found to exhibit excitation-dependent PL behaviors. With the excitation wavelength changed from 240 to 520 nm, the PL peak shifts to longer wavelength with the strongest peak at 520 nm when excited at 480 nm for N-GQDs-35. The emission spectra of the N-GQDs-35-10 also show a similar excitation-dependent feature, but the strongest peak is blue-shifted to 480 nm excited at 280 nm. PL excitation spectra (PLE) of N-GQDs-35 and N-GQDs-35-10 emissions indicate that different types of electronically excited states exist for the two cases, and the electron–hole recombination resulting from them brings about the PL (Figure S3, Supporting Information).[42] As a control, RN-GQDs-35 was prepared hydrothermally without ammonia for 10 h; blue PL was observed with the strongest peak at 462 nm excited at 365 nm (Figure 4a, inset). Previous reports revealed that different nitrogen atoms function in the graphene sheet by the hydrothermal method in the presence of ammonia solution.[43] As mentioned in the Introduction, different kinds of amino species will make significant contribution to the PL; for example, primary amino groups attached at the edge of sp^2 cluster will increase the electron density of GQDs and decrease the band gap, resulting in the red-shift of PL. While relatively strong electron withdrawing ability of pyridinic-N and pyrrolic-N atoms in the GQDs would bring about blue-shift of PL. Moreover, amino groups could act as an effective passivation agent to enhance the PL of the GQDs.[38]

X-ray photoelectron spectroscopy (XPS) characterizations are followed to analyze the elemental composition and nitrogen bonding configurations in N-GQDs. As seen in Figure 5a, the XPS shows a N_{1s} peak at ca. 401 eV and O_{1s} peak at 532 eV for N-GQDs. The N/C atomic ratio increases slightly from 6.0% (CF) to 6.5% (N-GQDs-35) and is maintained at a high level around 11.4% for the N-GQDs-35-10, while the O/C atomic ratios decrease from 43.8 to 33.3% for N-GQDs-35-10 compared with N-GQDs-35; however, the contents of O and N for both of them are still higher than that of the N-GQDs reported previously,[22] thus enabling the N-GQDs-35-10 high aqueous solubility. Figure 5b–e presents a comparison of the C_{1s} and N_{1s} high-resolution XPS spectra of as-prepared N-GQDs-35 and N-GQDs-35-10; the components of the C_{1s} spectrum of N-GQDs-35 located at 284.7, 285.3, 286.3, 288.4, and 289.0 eV can be assigned to C═C, C–OH, C–O–C, C═O, and COOH groups, respectively, while for N-GQDs-35-10, the components from C–O–C and COOH nearly disappear and the dominating peaks located at 285.9 eV could be ascribed to C–N bonds through nucleophilic reaction with ammonia. In N-GQDs-35, the high-resolution spectrum of N_{1s} shows the presence of pyridine-like (398.6 eV), pyrrolic (400.2 eV), and quaternary (401.7 eV) N atoms. Pyridinic N and pyrrolic N, respectively, devote one and two p-electrons to the π conjugated network, and quaternary N results from the substitution of C by N atoms in the hexagonal ring. Apart from these three nitrogen types, a shoulder peak around 405.8 eV is observed; the signal is presumably assigned to nitrogen oxides.[44] It can be noted that the nitric acid-treatment introduces not only a large amount of oxygenated functional groups but also a certain amount of nitrogen-containing groups onto N-GQDs, which must be related to the electrophilic substitution reaction between sp^2 C–H defects (especially at broken edges in the graphitic structure) and nitronium ions. After hydrothermal treatment of N-GQDs-35, the peak of

dx.doi.org/10.1021/am400415t | ACS Appl. Mater. Interfaces 2013, 5, 3362–3369

nitrogen oxides disappears. In N-GQDs-35-10, compared with RN-GQDs-35 (Figure S4, Supporting Information), an intensive peak appears at 399.5 eV, which is typically assigned to primary amines ($-NH_2$) bonded to the graphene.[24] Therefore, it is inferred that electron donation from the lone pair electrons of primary amines to the antibonding state in the benzene ring can increase electron density in the N-GQDs and decrease their band gaps, consequently leading to the red-shift of the PL emission of N-GQDs-35-10 compared with RN-GQDs-35.[25]

As discussed above, the multidimentional hybrid GQDs possess a high amount of N atoms and a large amount of holes and edges on the surface, which will bring about a higher electrochemical activity than sole basal plane. N-functioned carbon nanomaterials such as N-GQDs,[22] N-CNTs[45] and N-graphene[46] have been demonstrated to hold great promise as metal-free electrocatalysts to replace the commercially available Pt-based catalysts for the ORR. Thus, ORR experiments are performed, however, in contrast with the regular micrometer-sized GO colloids which tend to migrate to the water surface over time and eventually lead to a continuous GO thin film covering the surface of an evaporating droplet after drying. A droplet of N-GQDs tends to form the typical "coffee ring stain" type of drying pattern (Figure S5, Supporting Information), just like common water-soluble or dispersible materials. To avoid any possible "coffee ring stain" effect of N-GQDs on the glassy carbon (GC) base electrode (Figure S5, Supporting Information), we utilize an electrically conductive graphene assembly to support the N-GQDs as metal-free ORR catalysts. The graphene-supported N-GQDs-35-10 (N-GQDs-35-10/graphene) is prepared by hydrothermal treatment of a suspension of graphene oxides with N-RQDs-35-10 (Figure S6, Supporting Information). It is reported that this mild process ensured the formation of N-GQDs/graphene assemblies without acutely changing the intrinsically chemical nature of the N-GQDs.[22] As a control experiment, hydrothermal treatment of RN-GQDs-35/graphene oxides composites and sole graphene oxides is also carried out under the same condition. It is found that graphene oxide is self-assembled into hydrogel via hydrothermal reaction (Figure S7A, Supporting Information),[32] while N-RQDs/graphene composites could be homogeneously dispersed in water under ultrasound (Figure S7B, Supporting Information), facilitating even film forming on the surface of glassy carbon electrode. Thus, the effect from the glassy carbon (GC) base electrode could be avoided. The electrocatalytic activity of N-GQDs-35-10/graphene, RN-GQDs-35/graphene, graphene, and commercial Pt/C catalyst (40 wt % Pt on carbon black) for ORR is first examined by cyclic voltammetry (CV) in 0.1 M N_2 or O_2 saturated KOH solution. As shown in Figure 6a, a featureless capacitive current background is observed between −0.8 and +0.4 V for N-GQDs-35-10/graphene in the N_2-saturated solution. In contrast, a well-defined cathodic peak centered at −0.25 V emerges in the CV in the O_2-saturated solution, while graphene (Figure S8f, Supporting Information), RN-GQDs-35/graphene (Figure S9, Supporting Information), and commercial Pt/C catalyst (Figure 6b) show a negatively shifted peak potential at −0.36, −0.31, and −0.24 V, respectively. Moreover, the onset potentials, an important criterion to evaluate the activity of ORR catalyst, are −0.11, −0.19, −0.16, and −0.03 V for N-GQDs-35-10/graphene, RN-GQDs-35/graphene, graphene, and commercial Pt/C catalyst, respectively, as the electrolyte solution is saturated with O_2, hence suggesting a pronounced electrocatalytic activity of N-GQDs-35-10/graphene for oxygen reduction, close to those of the commercial Pt/C catalyst. To evaluate the properties of the new electrocatalyst, the crossover effect should be considered because the fuel molecules such as methanol and glucose in the anode sometimes permeate through the polymer membrane to the cathode and seriously affect the performance of the catalysts. Thus, the electrocatalytic sensitivity of N-GQDs-35-10/graphene and commercial Pt−C catalysts are measured against the electrooxidation of methanol in ORR. As shown in Figure 6a,b, a strong response is observed for the Pt−C catalyst in O_2-saturated 0.1 M KOH solution with 3 M methanol, whereas no noticeable response for N-GQDs-35-10/graphene is detected under the same conditions. Apparently, N-GQDs-35-10/graphene hybrids exhibit a high selectivity for ORR with a remarkably good tolerance of crossover effects. To gain further insight into the oxygen reduction reaction in N-GQDs-35-10/graphene hybrid, rotating disk electrode (RDE) voltammetry is performed in O_2-saturated 0.1 M KOH solution. Linear-sweep voltammetry (LSV) curves of the ORR for N-GQDs/graphene are shown in Figure 6c at different electrode rotation rates. The measured current density shows the typical increase with increasing rotation rate due to the enhanced diffusion of electrolytes.[47] The transferred electron number per O_2 molecule involved in the ORR process is determined using the Koutecky−Levich equation;[48] and the corresponding curves are plotted for different potentials in Figure 6d. The parallel and straight fitting lines imply a first-order reaction with respect to dissolved oxygen. The n value for N-GQDs-35-10/graphene is calculated to be 3.8−4.0 over the potential range from −0.4 to −0.7 V (Figure 6d, inset), suggesting a four-electron process for the ORR on the N-GQDs-35-10/graphene electrodes. We further tested the durability of N-GQDs-35-10/graphene, which is better than commercial Pt/C electrode after 1000 cycles in O_2-saturated 0.1 M KOH solution (Figure S10, Supporting Information). From these electrochemical characterizations, it can be seen that the catalytic performance of our novel hybrid is comparable to those reported previously,[22,49,50] and was not compromised by the scale-up.

CONCLUSION

In summary, we have developed a simple yet effective ammonia-mediated bond-scission strategy for generating a novel lotus seedpod surface-like multidimentional architecture of GQD hybrids with O- and N-rich functional groups, which shows favorable tuned PL property. Moreover, N-GQDs supported by graphene sheets have been demonstrated to possess superior metal-free electrocatalytic ability toward ORR. These results could provide useful information to further develop other novel N-GQDs with tailored PL and high activities for use in bioimaging, fuel cells, and various other electronic devices.

ASSOCIATED CONTENT

Supporting Information

The synthesis of GO, SEM images of the PAN-based carbon fibers, emission images of N-GQDs after hydrothermal treatment at varied temperatures, PLE spectra of N-GQDs-35 and N-GQDs-35-10, high-resolution N_{1s} peaks of RN-GQDs-35, "coffee ring stain" type of N-GQDs-35-10, TEM image of N-GQDs-35-10/graphene, and cyclic voltammograms of various N-GQDs and RN-GQDs-35/graphene. This informa-

tion is available free of charge via the Internet at http://pubs.acs.org/.

AUTHOR INFORMATION

Corresponding Author

*E-mail: peiyiwu@fudan.edu.cn. Tel: +86-21-65643255. Fax: +86-21-65640293.

Notes

The authors declare no competing financial interest.

ACKNOWLEDGMENTS

This work was financially supported by the National Basic Research Program of China (2009CB930000).

REFERENCES

(1) Cao, L.; Meziani, M. J.; Sahu, S.; Sun, Y. P. *Acc. Chem. Res.* **2012**, *46*, 171.
(2) Tao, H.; Yang, K.; Ma, Z.; Wan, J.; Zhang, Y.; Kang, Z.; Liu, Z. *Small* **2012**, *8*, 281.
(3) Markovic, Z. M.; Ristic, B. Z.; Arsikin, K. M.; Klisic, D. G. *Biomaterials* **2012**, *33*, 7084.
(4) Zhu, C.; Zhai, J.; Dong, S. *Chem. Commun.* **2012**, *48*, 9367.
(5) Son, D. I.; Kwon, B. W.; Park, D. H.; Seo, W. S.; Yi, Y.; Angadi, B.; Lee, C. L.; Choi, W. K. *Nat. Nano* **2012**, *7*, 465.
(6) Shen, J.; Zhu, Y.; Yang, X.; Li, C. *Chem. Commun.* **2012**, *48*, 3686.
(7) Li, L.; Wu, G.; Yang, G. H.; Peng, J.; Zhao, J.; Zhu, J. J. *Nanoscale* **2013**, DOI: 10.1039/C3NR33849E.
(8) Peng, J.; Gao, W.; Gupta, B. K.; Liu, Z. *Nano Lett.* **2012**, *12*, 844.
(9) Shinde, D. B.; Pillai, V. K. *Chem.—Eur. J.* **2012**, *18*, 12522.
(10) Pan, D.; Zhang, J.; Li, Z.; Wu, M. *Adv. Mater.* **2010**, *22*, 734.
(11) Li, L. L.; Ji, J.; Fei, R.; Wang, C. Z.; Lu, Q.; Zhang, J. R.; Jiang, L. P.; Zhu, J. J. *Adv. Funct. Mater.* **2012**, *22*, 2971.
(12) Zhou, X.; Zhang, Y.; Wang, C.; Wu, X.; Yang, Y.; Zheng, B.; Wu, H.; Guo, S.; Zhang, J. *ACS Nano* **2012**, *6*, 6592.
(13) Liu, R.; Wu, D.; Feng, X.; Müllen, K. *J. Am. Chem. Soc.* **2011**, *133*, 15221.
(14) Yan, X.; Li, B.; Li, L. S. *Acc. Chem. Res.* **2013**, DOI: 10.1021/ar300137p.
(15) Hamilton, I. P.; Li, B.; Yan, X.; Li, L. S. *Nano Lett.* **2011**, *11*, 1524.
(16) Dai, L. *Acc. Chem. Res.* **2012**, *46*, 31.
(17) Ponomarenko, L. A.; Schedin, F.; Katsnelson, M. I.; Yang, R.; Hill, E. W.; Novoselov, K. S.; Geim, A. K. *Science* **2008**, *320*, 356.
(18) Zhuo, S.; Shao, M.; Lee, S. T. *ACS Nano* **2012**, *6*, 1059.
(19) Li, Y.; Hu, Y.; Zhao, Y.; Shi, G.; Deng, L.; Hou, Y.; Qu, L. *Adv. Mater.* **2011**, *23*, 776.
(20) Zhao, J.; Chen, G.; Zhu, L.; Li, G. *Electrochem. Commun.* **2011**, *13*, 31.
(21) Zhu, S.; Zhang, J.; Qiao, C.; Tang, S.; Li, Y.; Yuan, W.; Li, B.; Tian, L.; Liu, F.; Hu, R.; Gao, H.; Wei, H.; Zhang, H.; Sun, H.; Yang, B. *Chem. Commun.* **2011**, *47*, 6858.
(22) Li, Y.; Zhao, Y.; Cheng, H.; Hu, Y.; Shi, G.; Dai, L.; Qu, L. *J. Am. Chem. Soc.* **2011**, *134*, 15.
(23) Li, Q.; Zhang, S.; Dai, L.; Li, L. S. *J. Am. Chem. Soc.* **2012**, *134*, 18932.
(24) Tetsuka, H.; Asahi, R.; Nagoya, A.; Okamoto, K.; Tajima, I.; Ohta, R.; Okamoto, A. *Adv. Mater.* **2012**, *24*, 5333.
(25) Jin, S. H.; Kim, D. H.; Jun, G. H.; Hong, S. H.; Jeon, S. *ACS Nano* **2013**, DOI: 10.1021/nn304675g.
(26) Cheng, H.; Zhao, Y.; Fan, Y.; Xie, X.; Qu, L.; Shi, G. *ACS Nano* **2012**, *6*, 2237.
(27) Skrabalak, S. E.; Au, L.; Li, X.; Xia, Y. *Nat. Protoc.* **2007**, *2*, 2182.
(28) Yavuz, M. S.; Cheng, Y.; Chen, J.; Cobley, C. M.; Zhang, Q.; Rycenga, M.; Xie, J.; Kim, C.; Song, K. H.; Schwartz, A. G.; Wang, L. V.; Xia, Y. *Nat. Mater.* **2009**, *8*, 935.
(29) Li, W.; Deng, Y.; Wu, Z.; Qian, X.; Yang, J.; Wang, Y.; Gu, D.; Zhang, F.; Tu, B.; Zhao, D. *J. Am. Chem. Soc.* **2011**, *133*, 15830.
(30) Fang, Y.; Lv, Y.; Che, R.; Wu, H.; Zhang, X.; Gu, D.; Zheng, G.; Zhao, D. *J. Am. Chem. Soc.* **2013**, DOI: 10.1021/ja310849c.
(31) Yan, X.; Li, Q.; Li, L. S. *J. Am. Chem. Soc.* **2012**, *134*, 16095.
(32) Xu, Y.; Sheng, K.; Li, C.; Shi, G. *ACS Nano* **2010**, *4*, 4324.
(33) Cao, Y.; Lai, Z.; Feng, J.; Wu, P. *J. Mater. Chem.* **2011**, *21*, 9271.
(34) Shin, Y. R.; Jung, S. M.; Jeon, I. Y.; Baek, J. B. *Carbon* **2013**, *52*, 493.
(35) Sugimoto, Y.; Pou, P.; Custance, O.; Jelinek, P.; Abe, M.; Perez, R.; Morita, S. *Science* **2008**, *322*, 413.
(36) Song, B.; Schneider, G. g. F.; Xu, Q.; Pandraud, G. g.; Dekker, C.; Zandbergen, H. *Nano Lett.* **2011**, *11*, 2247.
(37) Pan, D.; Guo, L.; Zhang, J.; Xi, C.; Xue, Q.; Huang, H.; Li, J.; Zhang, Z.; Yu, W.; Chen, Z.; Li, Z.; Wu, M. *J. Mater. Chem.* **2012**, *22*, 3314.
(38) Zhang, Z.; Wu, P. *CrystEngComm* **2012**, *14*, 7149.
(39) Lu, Y.; Jiang, Y.; Wei, W.; Wu, H.; Liu, M.; Niu, L.; Chen, W. *J. Mater. Chem.* **2012**, *22*, 2929.
(40) Pan, D.; Zhang, J.; Li, Z.; Wu, M. *Adv. Mater.* **2010**, *22*, 734.
(41) Kim, S.; Hwang, S. W.; Kim, M. K. *ACS Nano* **2012**, *6*, 8203.
(42) Zhu, S.; Zhang, J.; Tang, S.; Qiao, C.; Wang, L.; Wang, H.; Liu, X.; Li, B.; Li, Y.; Yu, W.; Wang, X.; Sun, H.; Yang, B. *Adv. Funct. Mater.* **2012**, *22*, 4732.
(43) Zhang, C.; Hao, R.; Liao, H.; Hou, Y. *Nano Energy* **2013**, *2*, 88.
(44) Flatt, A. K.; Chen, B.; Tour, J. M. *J. Am. Chem. Soc.* **2005**, *127*, 8918.
(45) Yu, D.; Xue, Y.; Dai, L. *J. Phys. Chem. Lett.* **2012**, *3*, 2863.
(46) Wu, G.; Mack, N. H.; Gao, W.; Ma, S.; Zhong, R.; Han, J.; Baldwin, J. K.; Zelenay, P. *ACS Nano* **2012**, *6*, 9764.
(47) Lin, Z.; Waller, G.; Liu, Y.; Liu, M.; Wong, C. P. *Adv. Energy Mater.* **2012**, *2*, 884.
(48) Lin, Z.; Song, M. k.; Ding, Y.; Liu, Y.; Liu, M.; Wong, C. P. *Phys. Chem. Chem. Phys.* **2012**, *14*, 3381.
(49) Yang, S.; Feng, X.; Wang, X.; Müllen, K. *Angew. Chem., Int. Ed.* **2011**, *50*, 5339.
(50) Sheng, Z. H.; Shao, L.; Chen, J. J.; Bao, W. J.; Wang, F. B.; Xia, X. H. *ACS Nano* **2011**, *5*, 4350.